J. Fluid Mech. (2003), *vol.* 493, *pp.* 345–361.
DOI: 10.1017/S0022112003005858 Printed in the United Kingdom

Topological chaos in inviscid and viscous mixers

By M. D. FINN, S. M. COX AND H. M. BYRNE

School of Mathematical Sciences, University of Nottingham, University Park, Nottingham NG7 2RD, UK

(Received 16 October 2002 and in revised form 29 May 2003)

Topological chaos may be used to generate highly effective laminar mixing in a simple batch stirring device. Boyland, Aref & Stremler (2000) have computed a material stretch rate that holds in a chaotic flow, provided it has appropriate topological properties, irrespective of the details of the flow. Their theoretical approach, while widely applicable, cannot predict the size of the region in which this stretch rate is achieved. Here, we present numerical simulations to support the observation of Boyland *et al.* that the region of high stretch is comparable with that through which the stirring elements move during operation of the device. We describe a fast technique for computing the velocity field for either inviscid, irrotational or highly viscous flow, which enables accurate numerical simulation of dye advection. We calculate material stretch rates, and find close agreement with those of Boyland *et al.*, irrespective of whether the fluid is modelled as inviscid or viscous, even though there are significant differences between the flow fields generated in the two cases.

1. Introduction

Static and dynamic mixing devices are important in many industries, e.g. food production (Prakash & Kokini 2000), controllable manufacture of polymer blends and composites (Zumbrunnen & Inamdar 2001), and biological scenarios, such as ventilation (Butler & Tsuda 1997) and digestion (Macagno & Christensen 1980). However, techniques for understanding or producing effective fluid mixers, while highly advanced, remain far from complete, for three reasons: theories of chaos and turbulence are themselves incomplete; well-resolved numerical simulation of the intricacies of mixing remains a significant computational challenge; and accurate expressions for the flow field in practical stirring devices are rare.

A significant recent theoretical advance concerns the concept of 'topological chaos' (Ricca & Berger 1996; Boyland, Aref & Stremler 2000; MacKay 2001; Boyland 2002; Boyland, Stremler & Aref 2003): without reference to any computation or exact flow details, Boyland *et al.* (2000) have demonstrated, in an unusual blend of *ad hoc* experimentation and abstract mathematics, that flows with the topology of certain braids achieve a material stretch rate which can be determined quantitatively, given only the topology of the flow. However, a key feature not predicted by their theoretical considerations is the size of the domain in which this stretch rate is attained. Indeed, according to the theory, this domain may have measure zero, and if this were the case then the theory would have little practical impact. Here we provide numerical results that support the observations of Boyland *et al.*, that the chaotic region is in fact commensurate with the region of fluid through which the stirring elements move during operation of the device. We should make clear at the outset that we use the terminology 'topological chaos' in the same sense as Boyland *et al.* (2000), to

mean 'complexity that cannot be removed by continuous deformations of the shape of the fluid region, or by continuous modification in the actual trajectories of the stirrers', and not in the sense of 'strong topological mixing' from ergodic theory, for example (Pollicott & Yuri 1998). By adopting such usage consistently, we hope that no confusion can arise. We furthermore note that the definition of how one should measure the quality of mixing achieved by a fluid flow is by no means unique – we shall compute the stretch rate of a finite material line, but many other measures are routinely used, including measurement of the degree of chaotic motion in the Poincaré section (Aref & Balachandar 1986; Jones, Thomas & Aref 1989), the calculation of Liapunov exponents (Muzzio & Swanson 1991), the return percentage of diffusive tracer particles (Aref & Jones 1989), the growth rate of intermaterial density (Muzzio *et al.* 1999; Giona & Adrover 2001), and the distribution of lamellae generated by mixing a blob of fluid (Clifford, Cox & Roberts 1998, 2000; Metcalfe & Ottino 1994; Muzzio & Ottino 1989, 1990; Sawyers, Sen & Chang 1996).

Of course, there are many devices in which excellent chaotic mixing can be achieved without using topological chaos, however the mixing quality is measured: for analytical and numerical convenience, most investigations have focused on the slow, Stokes flow regime – examples for which the corresponding exact velocity field is known include the translating rotating mixer (Finn & Cox 2001), the double journal bearing flow (Jana, Metcalfe & Ottino 1994), the rotated arc mixer (Rudman *et al.* 2001), and the partitioned pipe mixer (Kusch & Ottino 1992; Meleshko *et al.* 1999) used to model the Kenics static mixer. However, for each of these devices, the quality of mixing depends on a careful tuning of the system parameters. The concept of topological chaos offers at least the prospect of building into a mixer design some lower bound on mixing quality, but further investigation of the practicalities is required, as described here.

In this paper we study a batch stirring device (BSD), in which an arbitrary number of cylindrical rods of circular cross-section move independently to stir a fluid (Boyland *et al.* 2000). In order to generate topological chaos in such a device, it is necessary to have three or more stirring rods. The generation of a chaotic flow in a BSD with fewer stirring rods is, of course, perfectly possible (Finn & Cox 2001), but ensuring that the chaotic region is of substantial size relies on a tuning of the parameters. We investigate below the extent to which increasing the number of stirring rods, and the consequent introduction of topological chaos, improves the mixing.

We construct the velocity field for two-dimensional flow in the BSD, for either an inviscid fluid or Stokes flow in a viscous fluid. When there is only a single stirring element, it is possible to construct the exact velocity field for Stokes flow in closed form (Finn & Cox 2001) using finitely many terms, by means of image systems of singularities (Avudainayagam & Jothiram 1988; Sen 1989); however, we have found that attempts to derive the corresponding velocity field with multiple stirring elements lead to insurmountable analytical difficulties. The alternative series solution adopted here is based on an approach due to Price, Mullin & Kobine (2003) and L. N. Trefethen (personal communication). We construct series which converge extremely rapidly, thus giving rise to excellent truncations for numerical purposes. This technique is fast and easy to implement and allows accurate simulations of chaotic advection. Vikhansky (2003) has computed some corresponding flows with three stirring rods using the 'immersed boundary method': these illustrate the chaotic motion of fluid particles in a BSD, but a corresponding level of accuracy is difficult to achieve in his simulations, or indeed any which use a finite-element or finite-difference approach.

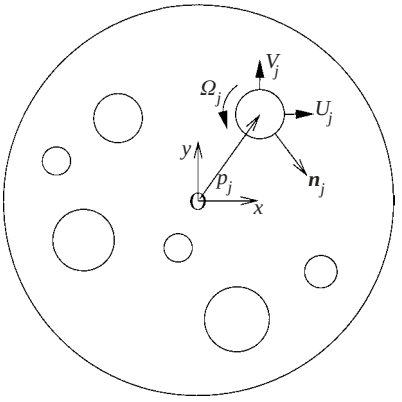

FIGURE 1. Geometry of the BSD. Here, x and y are Cartesian coordinates. Two-dimensional flow is driven by m circular cylinders, each centred at $z = p_j$ (where $z = x + \mathrm{i}y$), with radius a_j, translating with velocity (U_j, V_j) and (for the viscous model only) rotating anticlockwise about its axis with angular speed Ω_j. The unit normal of the jth cylinder is $\boldsymbol{n}_j$. The fluid is enclosed between the internal cylinders and an outer circular cylinder centred at $z = 0$, with radius a.

The remainder of this paper is structured as follows. In § 2, we describe the BSD, and our algorithm for calculating the corresponding velocity field. In § 3, we summarize key results from the topological theory, and in § 4, we present numerical stirring simulations which allow comparison with the abstract theory of Boyland *et al.* (2000). Discussion of some practicalities of mixer design and conclusions are given in §§ 5, and 6, respectively.

2. Mathematical models for the batch stirring device (BSD)

The BSD geometry (Boyland *et al.* 2000) is shown in figure 1. Flow is two-dimensional, in the (x, y)-plane. We shall develop inviscid and viscous models for the flow: in both it proves convenient to work with complex coordinates $z = x + \mathrm{i}y$ and $\bar{z} = x - \mathrm{i}y$, where x and y are Cartesian coordinates as indicated in the figure. We assume that there are m infinitely long circular cylinders placed in the fluid, with their axes at $z = p_j(t)$ and with radii a_j $(j = 1, \ldots, m)$. Each cylinder may move independently with a prescribed velocity $U_j + \mathrm{i}V_j = \mathrm{d}p_j/\mathrm{d}t$ and, in the case of the viscous model only, may rotate about its axis with angular speed $\Omega_j(t)$. The flow domain is finite, the cylinders being enclosed in the region $|z| \leqslant a$. Mixing is achieved by moving the m cylinders, and hence varying the geometry of the flow domain, in a time-periodic fashion.

In order to simulate mixing numerically, we must track with high accuracy the motion of inertialess tracer particles as they are advected with the fluid. It is therefore advantageous to have available an exact expression for the fluid velocity field, which allows evaluation of the velocity at an arbitrary point in the flow domain (rather than, say, a finite-difference approximation, where some interpolation is, in general, required). Unfortunately, for $m > 1$, such an exact expression is not available in closed form, so instead we calculate series solutions whose coefficients are then determined by computing the least-squared-error in the boundary conditions, subject to certain constraints, detailed later. The series converge rapidly, and so only a small number of terms need be taken in a numerical truncation.

2.1. *Inviscid irrotational model*

Our first model for the BSD is of incompressible inviscid irrotational flow. Here, it is most convenient to work with the complex potential $w = \phi + \mathrm{i}\psi$, where ϕ and ψ are, respectively, the velocity potential and streamfunction, the corresponding fluid velocity field (u, v) being obtained from

$$u - \mathrm{i}v = \frac{\mathrm{d}w}{\mathrm{d}z}. \tag{2.1}$$

The boundary conditions on the internal cylinders are

$$(u, v)\cdot\boldsymbol{n}_j = (U_j, V_j)\cdot\boldsymbol{n}_j \quad \text{on } |z - p_j| = a_j \quad (j = 1, \ldots, m), \tag{2.2}$$

where $\boldsymbol{n}_j$ is the unit normal vector of the jth cylinder (see figure 1). We also impose the no-penetration condition that

$$(u, v)\cdot\boldsymbol{n} = 0 \quad \text{on } |z| = a, \tag{2.3}$$

where $\boldsymbol{n}$ is the unit normal of the bounding cylinder.

We automatically satisfy (2.3) by using the Milne-Thomson circle theorem (Milne-Thomson 1968; Acheson 1996), so that w takes the form

$$w = f(z) + \overline{f(a^2/\bar{z})}, \tag{2.4}$$

for some analytic function $f(z)$.

Following Price *et al.* (2003), we seek a complex potential in the form

$$\begin{aligned} w = &\sum_{j=1}^{m}\left\{b_{j,1}\log(z - p_j) + \sum_{k=2}^{n} b_{j,k}(z - p_j)^{1-k}\right\} \\ &+ \sum_{j=1}^{m}\left\{\bar{b}_{j,1}(\log(z - q_j) + \log(-\bar{p}_j/a)) + \sum_{k=2}^{n}\bar{b}_{j,k}\left(\frac{a^2}{z} - \bar{p}_j\right)^{1-k}\right\}, \end{aligned} \tag{2.5}$$

which is consistent with (2.4), and hence automatically satisfies (2.3), where $q_j = a^2/\bar{p}_j$ and the $b_{j,k}$ are mn complex constants. (The exact solution is obtained in the limit $n \to \infty$.) Since there is no net source of fluid inside any internal cylinder, each $b_{j,1}$ is purely imaginary. Then, by the Kelvin circulation theorem, each $b_{j,1}$ must remain constant during the operation of the device; we choose $b_{j,1} = 0$, which corresponds to starting the system from rest, although other fixed circulations could be imposed.

The coefficients $b_{j,k}$ are found by minimizing the squared error in the boundary conditions (2.2) on the internal cylinders (Bourot 1969); recall that, by construction, the condition (2.3) on the outer cylinder is satisfied automatically. A sample of streamline plots for this model is shown in figure 2.

2.2. *Viscous model*

We now suppose that instead the BSD is filled with incompressible Newtonian viscous fluid. We consider Stokes flow, at vanishing Reynolds number, so that the streamfunction $\psi(z, \bar{z})$ satisfies the biharmonic equation $\nabla^4\psi = 0$ (Lamb 1932), and the velocity field may be obtained using

$$u + \mathrm{i}v = -2\mathrm{i}\frac{\partial\psi}{\partial\bar{z}}. \tag{2.6}$$

We aim to satisfy the no-slip boundary conditions

$$u + \mathrm{i}v = U_j + \mathrm{i}V_j + \mathrm{i}\Omega_j(z - p_j) \quad \text{on } |z - p_j| = a_j \quad (j = 1, \ldots, m) \tag{2.7}$$

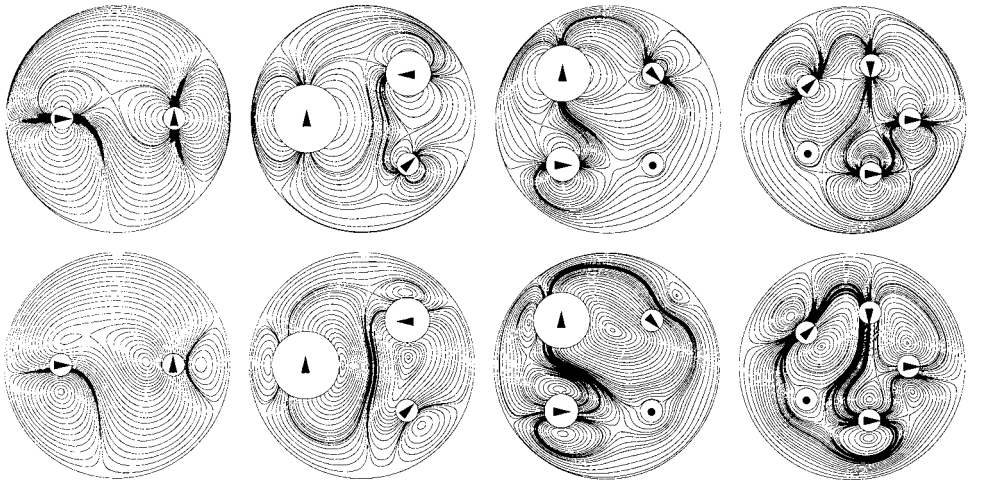

FIGURE 2. Illustrative plots showing instantaneous streamlines for the inviscid (upper row) and viscous (lower row) models. The two plots in each column correspond to identical cylinder positions and velocities (with directions indicated by arrows), allowing the two flow regimes to be compared. In each case, all cylinders have zero angular velocity about their respective axes.

and

$$u + \mathrm{i}v = 0 \quad \text{on } |z| = a. \tag{2.8}$$

Note that, in addition to the translational velocities of the stirring rods, their rotational velocities now also influence the flow field. Although rotation of a rod about its axis does not influence the topology of the flow, it does provide an additional degree of freedom for tuning parameters to optimize mixing performance.

We can satisfy (2.8) automatically by using the circle theorem for the biharmonic equation (Frazer 1925; Avudainayagam & Jothiram 1988; Sen 1989). Following Finn & Cox (2001), we find that the appropriate streamfunction involves placing rotlet and Stokeslet singularities, together with Laurent series, at the centre of each internal cylinder, and then applying the circle theorem to give a streamfunction of the form

$$\begin{aligned}\psi = &\sum_{j=1}^{m}\left\{ b_{j,1}\left[\tfrac{1}{4}\bar{z}\log\frac{q_j|z-p_j|^2}{p_j|z-q_j|^2} + \frac{|z|^2-a^2}{4|p_j|^2|z-q_j|^2}(\bar{p}_j\bar{z}(z+p_j) - a^2(\bar{z}+\bar{p}_j))\right]\right.\\ &\left. + \sum_{k=2}^{n} b_{j,k}[\bar{z}(z-p_j)^{1-k} + ((p_j+(k-1)z)\bar{z} - a^2k)(-p_j)^{-k}\bar{z}^k(\bar{z}-\bar{q}_j)^{-k}]\right\}\\ &+ \sum_{j=1}^{m}\left\{ c_{j,1}\left[\tfrac{1}{4}\log\frac{|q_j||z-p_j|^2}{|p_j||\bar{z}-\bar{q}_j|^2} + \frac{(|z|^2-a^2)(|z|^2-|q_j|^2)}{4a^2|z-q_j|^2}\right]\right.\\ &\left. + \sum_{k=2}^{n} c_{j,k}[(z-p_j)^{1-k} + ((p_j+(k-1)z)\bar{z} - a^2k)(-p_j)^{-k}\bar{z}^{k-1}(\bar{z}-\bar{q}_j)^{-k}]\right\}\\ &+ \text{c.c.},\end{aligned} \tag{2.9}$$

where c.c. denotes the complex conjugate of all preceding terms. In order to avoid a

singularity at the origin, we impose the constraint

$$\mathrm{Im} \sum_{j=1}^{m} c_{j,1} = 0. \tag{2.10}$$

As in § 2.1, the coefficients (here $b_{j,k}$ and $c_{j,k}$) may be determined by minimizing the squared error in (2.6), subject to (2.9); see figure 2.

2.3. *Features of the inviscid and viscous models*

Typical streamline plots for the BSD using the inviscid and viscous models and with up to five stirring rods are shown in figure 2. It is not our intention here to undertake a discussion of all possible flow topologies (see Price *et al.* 2003 for such a discussion with $m = 2$); however, we make some general remarks.

We note that there are two main differences between the inviscid and viscous streamline plots. First, in the inviscid case, the fluid motion is more localized, because the fluid slips around the moving cylinders; by contrast, the corresponding viscous fluid motion is more uniform, with the fluid speed being of the same order over much of the domain. One consequence of this difference is that material stretching in the inviscid BSD is also more localized than in the viscous BSD; consequently, it is more problematic to perform accurate numerical simulation of the advection of a fluid interface, for example, in the inviscid case. The second significant difference between the inviscid and viscous flows is the nature of the stagnation points. In an inviscid flow, stationary points are always hyperbolic, because the streamfunction satisfies Laplace's equation, and so cannot have internal extrema, whereas the viscous streamfunction satisfies the biharmonic equation, which allows both elliptic and hyperbolic stationary points. So, while some broad features of the flow field are the same in both inviscid and viscous models, it seems clear that if the internal cylinders execute a given motion then the details of the streamlines for the two models will be quite different. This underlines the remarkable nature of the results of Boyland *et al.* (2000), which depend on the topology of the boundary motions, but not on the detailed flow field.

For the purpose of numerical simulations, we find that taking $n = 10$ terms reduces the error in the velocity field (compared with an 'exact' solution obtained using the 'effectively infinite' value $n \approx 15$) below that introduced by time discretization, described later. The limit of machine precision is typically reached with $n \approx 15$ (working in Matlab, to 16 decimal places), and we find it straightforward to reduce errors to $O(10^{-9})$ before encountering conditioning difficulties with the least-squares problem. By comparison, Vikhansky (2003) reports errors of $O(10^{-4})$ for his finite-difference immersed-boundary simulations, although his method has the significant advantage of allowing extension to finite Reynolds number, which ours does not.

3. Theoretical background

In this section, we review some basics of braid notation, which provide a framework for our subsequent analysis of stretch rates for flows in the BSD with various topologies. We examine different ways of moving the internal cylinders ('stirring protocols') and evaluate their effectiveness in stretching material line elements.

Chaotic flows are characterized by the exponential stretching in time of material line elements, and the aim in previous studies of chaotic advection has often been to maximize the stretch rate by appropriate selection of the system parameters. However, the theoretical results of Boyland *et al.* (2000) yield a stretch rate generated by the motion of $m \geqslant 3$ cylinders without explicit reference to the underlying equations

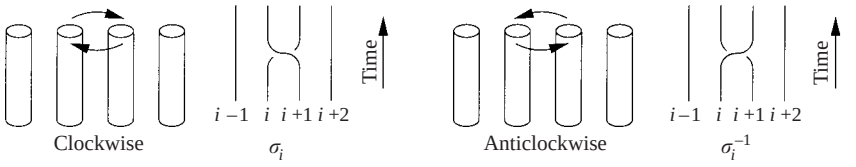

FIGURE 3. Braid diagrams illustrating the exchange in position of two adjacent cylinders. Neighbouring cylinders may interchange positions in either a clockwise or anticlockwise sense, characterized by braid letters σ_i or σ_i^{-1}, respectively. In the braid diagram corresponding to a clockwise exchange σ_i, the $(i+1)$th strand crosses over the ith strand, whereas for the braid letter σ_i^{-1}, the $(i+1)$th strand crosses beneath the ith strand.

governing the fluid motion. It should be emphasized that, at present, the great generality of the theory comes at a cost: the size of the region in which this stretch rate is achieved is unknown, and typically depends on the governing fluid equations; it may even have zero measure. It is our goal, therefore, to investigate the quality of mixing due to various stirring protocols, according to the fluid models outlined above, particularly noting the size of the chaotic region.

3.1. *Braid notation*

We assume that the stirring motion is periodic in time, with period T. At the beginning and end of any period, the axes of the m internal cylinders lie on the diameter $y=0$ of the outer cylinder. During the course of the stirring, pairs of adjacent cylinders are interchanged. Boyland *et al.* (2000) have described how such motion, when considered appropriately, has the topology of a physical braid on m strings, which in turn corresponds to a mathematical braid (Tufillaro, Abbot & Reilly 1992). To see how the mathematical theory of braids may be applied to the mixing problem, we begin by assigning to each interchange a braid letter σ_j or σ_j^{-1} (see figure 3). The subscript j indicates which two (adjacent) cylinders are interchanged, from $j=1$, which represents the left-most pair, to $j=m-1$, which represents the right-most pair. A superscript of -1 indicates that the cylinders orbit one another in an anticlockwise sense; no superscript indicates a clockwise orbit.

The sequence of interchanges during one complete period is the stirring protocol, and can be characterized by a braid word, which is a string of braid letters. Interchanges are made corresponding to each braid letter in sequence, reading from right to left. For example, the braid word $\sigma_1\sigma_2^{-1}$ means that we first interchange the second and third cylinders in an anticlockwise sense, then interchange the first and second cylinders in a clockwise sense. A braid word may also be represented schematically by a braid diagram, as shown in figure 3. Here, each line represents one of the m internal cylinders and time progresses from the bottom to the top of the diagram; each crossing of the lines represents an interchange of neighbouring cylinders.

Once we have selected the stirring protocol and the paths that cylinders take during their interchanges, we can simulate the corresponding fluid mixing, by tracking the advection of passive tracer particles in the flow. Since the stirring protocol is repeated periodically, it is efficient to store the series coefficients for the velocity field at a large number of time steps, so that they can be computed just once, prior to simulation. So it is significant that our method of solution is not only faster and more accurate than alternative finite-element or finite-difference techniques, but it also requires less storage: we need store only the series coefficients, rather than the velocity field itself at a full set of grid points. Other model simplifications allow

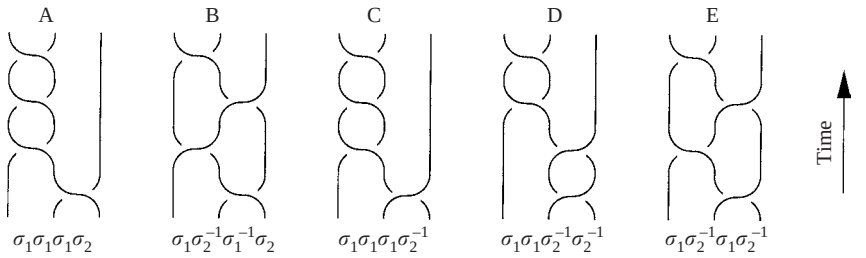

FIGURE 4. Braid diagrams and braid words for the five test protocols. Protocol A is 'finite-order' and does not have the correct topology to ensure effective stirring. Protocols B–E are 'pseudo-Anosov' and each have a (distinct) value of λ_{theory}; these protocols illustrate all possible values of this quantity that correspond to braid words of four letters.

us to reduce the computational and storage requirements further: if the cylinders have equal radius and are placed symmetrically either side of the origin $z = 0$, and if 'reasonable' interchanges are used, then reflectional and time-reversal symmetries may be invoked, so that with m cylinders, only $\lceil \frac{1}{2}(m-1) \rceil$ 'half-interchanges' need be calculated (where $\lceil \xi \rceil$ means the least integer not less than ξ).

3.2. *Theoretical prediction of a material stretch rate*

Using Thurston–Nielson theory, Boyland *et al.* (2000) have shown that the action of each braid letter in a stirring protocol is intimately linked with a matrix derived from its braid (Burau) matrix. In particular, for $m = 3$, a certain stretch rate given by the stirring action of a particular braid letter is predicted by the spectral radius (magnitude of the largest eigenvalue) of its associated matrix. The matrices corresponding to the braid letters σ_1, σ_1^{-1}, σ_2, σ_2^{-1} are, respectively (Boyland *et al.* 2000),

$$\mathbf{s}_1 = \begin{bmatrix} 1 & -1 \\ 0 & 1 \end{bmatrix}, \quad \mathbf{s}_1^{-1} = \begin{bmatrix} 1 & 1 \\ 0 & 1 \end{bmatrix}, \quad \mathbf{s}_2 = \begin{bmatrix} 1 & 0 \\ 1 & 1 \end{bmatrix}, \quad \mathbf{s}_2^{-1} = \begin{bmatrix} 1 & 0 \\ -1 & 1 \end{bmatrix}. \tag{3.1}$$

The matrix corresponding to the action of a braid word may be found be taking the matrix product of the component braid matrices, so that, for example, the protocol $\sigma_1\sigma_1\sigma_2^{-1}\sigma_2^{-1}$ has the braid matrix

$$\mathbf{s}_1\mathbf{s}_1\mathbf{s}_2^{-1}\mathbf{s}_2^{-1} = \begin{bmatrix} 1 & -1 \\ 0 & 1 \end{bmatrix}\begin{bmatrix} 1 & -1 \\ 0 & 1 \end{bmatrix}\begin{bmatrix} 1 & 0 \\ -1 & 1 \end{bmatrix}\begin{bmatrix} 1 & 0 \\ -1 & 1 \end{bmatrix} = \begin{bmatrix} 5 & -2 \\ -2 & 1 \end{bmatrix}, \tag{3.2}$$

which has spectral radius $\lambda_{\text{theory}} = 3 + 2\sqrt{2}$. If the BSD is operated according to this protocol, there is at least one material line whose length $l(t)$ grows at least as rapidly as

$$l(t)/l(0) \sim \lambda_{\text{theory}}^{t/T}, \tag{3.3}$$

where T is the period. According to the theory, only the flow topology matters, and this is completely characterized by the braid word. The nature of the flow, for example, whether it is inviscid or viscous, incompressible or compressible, does not matter: while the stretch rate λ_{theory} is the same in each case, the size and location of the appropriate region in which the stretch rate is achieved depend on the details of the flow.

Using the models from § 2, we are able to illustrate the predictions of Boyland *et al.* (2000) in numerical simulations of both inviscid and viscous models for the BSD. For the case $m = 3$, we have chosen five protocols, labelled A–E (see figure 4). Their braid words contain four letters, but give rise to different values of λ_{theory} (see table 1). Protocol A is special because its braid is topologically equivalent to the 'identity'

Protocol	Braid word	λ_{theory}	λ_{num}
A	$\sigma_1\sigma_1\sigma_1\sigma_2$	—	2.2
B	$\sigma_1\sigma_2^{-1}\sigma_1^{-1}\sigma_2$	$\frac{1}{2}(3+\sqrt{5}) \approx 2.6$	2.8
C	$\sigma_1\sigma_1\sigma_1\sigma_2^{-1}$	$\frac{1}{2}(5+\sqrt{21}) \approx 4.8$	5.0
D	$\sigma_1\sigma_1\sigma_2^{-1}\sigma_2^{-1}$	$3+2\sqrt{2} \approx 5.8$	5.8
E	$\sigma_1\sigma_2^{-1}\sigma_1\sigma_2^{-1}$	$\frac{1}{2}(7+3\sqrt{5}) \approx 6.9$	7.1

TABLE 1. Table of stretch rates for the five test protocols A–E. Indicated are λ_{theory}, together with numerical results λ_{num} based on our viscous model.

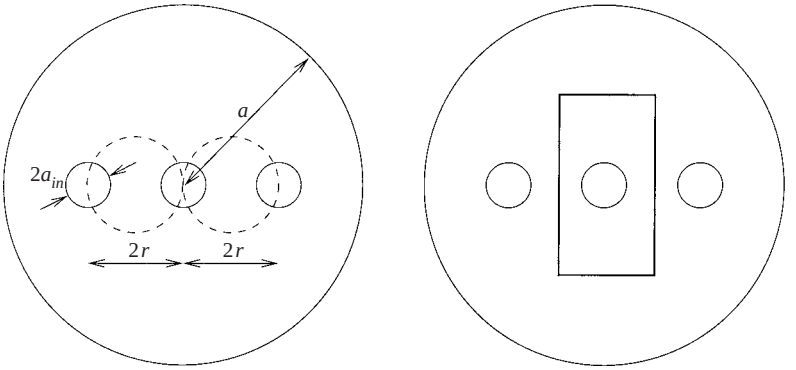

FIGURE 5. The BSD geometry at the start of a period, illustrated for $m = 3$. The internal cylinders all have radius a_{in}, and are equally spaced along the line $y = 0$, configured symmetrically. The distance between neighbouring cylinder axes is $2r$. When two adjacent cylinders are interchanged, they are moved along circular arcs of radius r centred on the mid-point between the two cylinders, either clockwise or anticlockwise. The right-hand diagram shows the initial position of the streak of dye.

braid, for which the crossings can be untied (see Boyland *et al.* 2000). Although we expect it might stir effectively in practice if its physical parameters are chosen appropriately, its braid matrix has complex eigenvalues, and so the topological theory does not guarantee exponential stretching of a material interface. Protocols B–E have non-trivial topology; in fact, they correspond to the four distinct values of λ_{theory} that can be generated by four-letter braid words.

4. Numerical simulations of dye advection

We have carried out numerical simulations of passive dye advection for protocols A–E. Initially, the axes of the cylinders are equi-spaced along the line $y = 0$; the cylinders are taken to be of equal radius, symmetrically placed about the origin, with the axes of neighbouring cylinders separated by a distance $2r$ (see figure 5). We investigate the parameter regime $a_{\text{in}}/a = 0.1$ (where a_{in} is the radius of each cylinder) and $r/a = 0.25$. A streak of dye is initially placed along the perimeter of a rectangle joining the four points with coordinates $(\pm a/4, \pm a/2)$, and is then advected by the fluid. When two adjacent cylinders are interchanged, we move them along circular arcs of radius r centred on the mid-point between their axes, so that the two

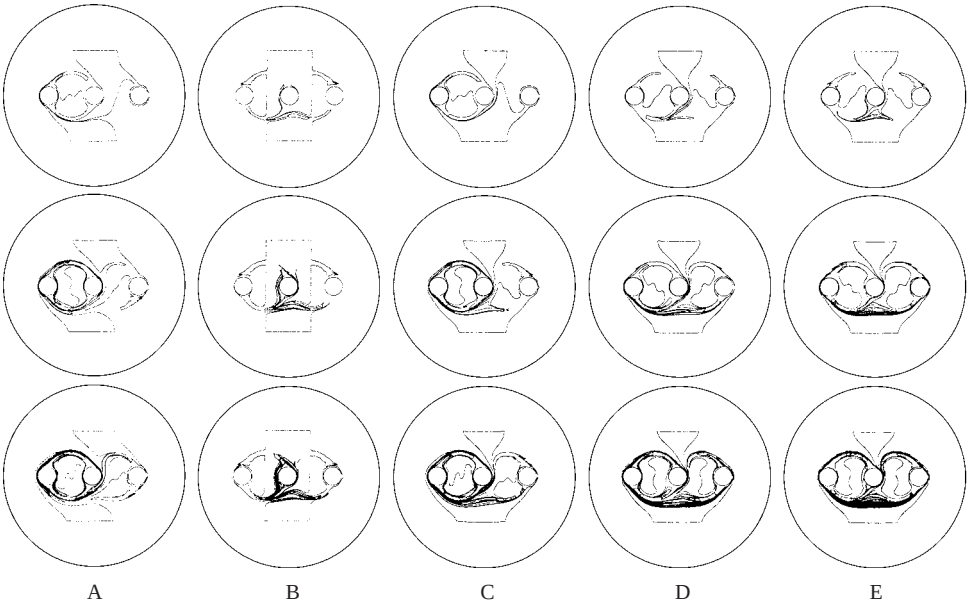

FIGURE 6. Numerical dye-advection simulations of the five test protocols A–E in the inviscid model. The protocols are labelled by column. The rows show the dye location after (from top to bottom) 1, 2 and 3 periods of the flow.

cylinders remain at all times on opposite ends of a diameter. During this procedure, the cylinders themselves do not rotate about their axes.

Results for the inviscid and viscous models of the BSD are shown in figures 6 and 7, respectively. One striking difference between the two sets of results is that the inviscid flow generates structures that are less smooth than the viscous flow. This feature is due to the greater localization of the inviscid flow. A second notable feature is that the dye is taken to different parts of the flow domain in the two models, most evidently for protocols C, D and E. Broadly speaking, the dyed fluid is predominantly moved into the region $y < 0$ in the viscous model, whereas its distribution is more symmetrical between upper and lower halves of the domain in the inviscid case. An explanation for this feature can be found by examining the velocity fields generated by the braid letters σ_1 and σ_2^{-1}, of which the protocols C, D and E are composed. Each of these braid letters involves either the leftmost or the rightmost internal cylinder exchanging places with the central cylinder, with the latter moving through the region $y < 0$ while the other moves through $y > 0$. We find that in the viscous model, such a motion tends by entrainment to generate a net motion of fluid in the central region in the negative y-direction and a net motion in the positive y-direction along the outer cylinder wall. By contrast, there is no such entrainment in the inviscid model. Thus, after a small number of stirring periods, the dyed fluid, which is initially predominantly in the central region, is moved into the region $y < 0$ in the viscous model, while there is no such marked drift in the inviscid model, as seen in figures 6 and 7. If the motion were followed for a longer time, the viscous dyed fluid would explore both $y < 0$ and $y > 0$. Indeed, this is demonstrated in protocol C: we note that whereas protocols D and E involve σ_1 and σ_2^{-1} in equal measure, C involves predominantly σ_1; these additional exchanges on the left-hand

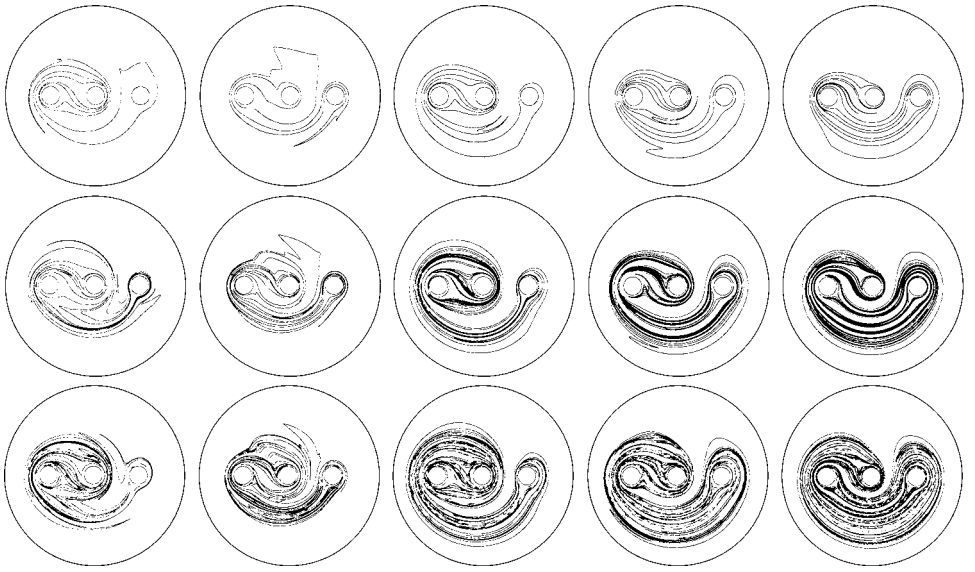

FIGURE 7. Numerical dye-advection simulations of the five test protocols A–E in the viscous model. The protocols are labelled by column. The rows show the dye location after (from top to bottom) 1, 2 and 3 periods of the flow.

side of the fluid domain can clearly be seen in figure 7 to have moved the fluid there into both upper and lower halves of the domain.

Despite the significant qualitative differences between the locations of the stretched dye-streaks in the two models, in each case the region of good mixing is eventually commensurate with the entire region through which the internal cylinders are moved (cf. Boyland *et al.* 2000).

We have computed the time variation in the length of the dye-streak, according to the viscous model, and evaluated the corresponding stretch rate for each protocol; our results are shown in table 1. If the length of the dye-streak is $l(t)$ at time t, then we define the numerical stretch rate λ_{num} to be the best fit to the expression

$$\lambda_{\mathrm{num}}^{t/T} = l(t)/l(0).$$

In tracking the exponentially growing dye-streak, we have used the dynamic particle insertion algorithm of Krasnopolskaya *et al.* (1999) to ensure that it remains well resolved. There is close agreement between $\lambda_{\mathrm{theory}}$ and λ_{num}. We interpret this as indicating that the results of Boyland *et al.* (2000) are a good predictor of the stretch rate of a finite material line (although clearly the possibility remains that the agreement found here is fortuitous and that in other flows the agreement would be less good). It should be noted that the initial dye-streak does not seem to lie entirely in a chaotic region. Therefore, some section of it stretches subexponentially. However, the influence of any such section on the value of λ_{num} diminishes with time (since it occupies an increasingly small fraction of the total length of the dye-streak). Corresponding calculations of the stretch rate for the inviscid model are not presented, because we have found it difficult to compute with accuracy the interface length in this case, due to the highly localized stretching. Although we have less confidence in the inviscid results, they yield stretch rates consistent with those given in table 1.

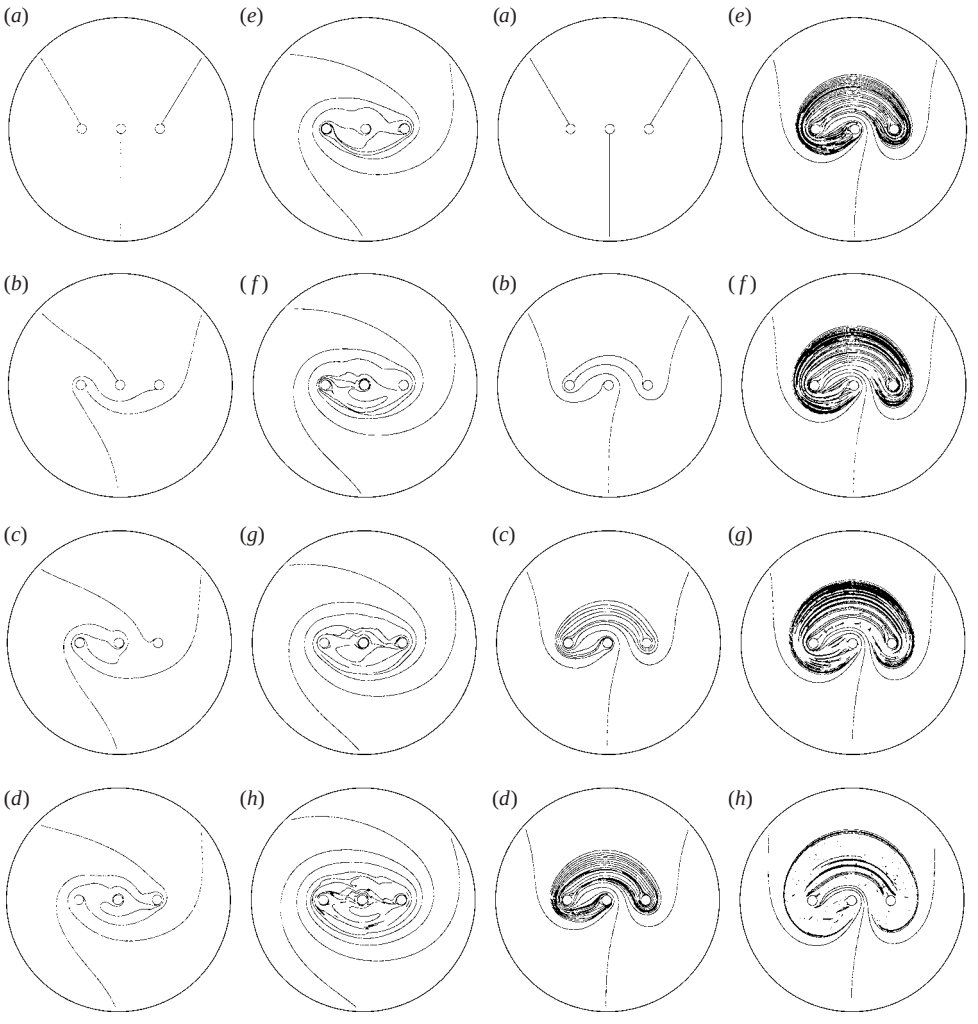

FIGURE 8. Numerical dye-advection simulations in the viscous model with $m = 3$, under motions corresponding to $(\sigma_1\sigma_2)^p$ (left) and $(\sigma_1^{-1}\sigma_2)^p$ (right). Here $a_{\text{in}}/a = 0.043$ and $r/a = 0.17$, roughly in accordance with the experimental conditions of Boyland *et al.* (2000). Configuration at (*a*) $p = 0$; (*b*) $p = 1$; (*c*) $p = 2$; (*d*) $p = 3$; (*e*) $p = 4$; (*f*) $p = 5$; (*g*) $p = 6$ and (*h*) $p = 9$.

Finally, we present in figure 8 numerical simulations of the viscous model corresponding to the experiments reported by Boyland *et al.* (2000). These results may be compared with their figure 2, which shows the result of stirring by motions $(\sigma_1\sigma_2)^p$ and $(\sigma_1^{-1}\sigma_2)^p$ in our notation (respectively, f^p and g^p in their notation), for $p = 0, 1, 2, 3, 4, 5, 6, 9$. The agreement between simulation and experiment is excellent.

5. Some practicalities of designing a batch stirring device

We now discuss some of the practicalities of building a mechanical BSD that generates topological chaos. Although the use of robotics for moving the cylinders would provide great flexibility, and allow the protocol to be changed easily, it is feasible, and more straightforward, to achieve effective stirring topologies using simple systems of gearing. For instance, with $m = 3$, only one cylinder need be moved to

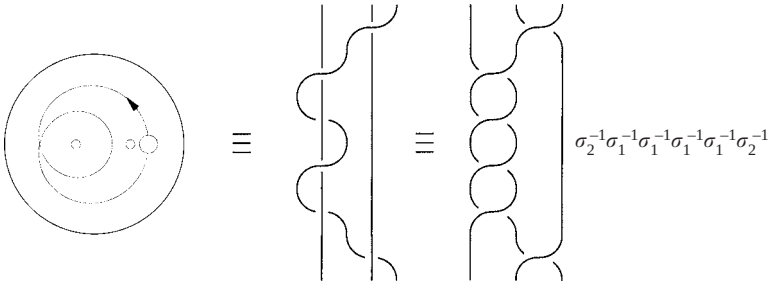

FIGURE 9. A stirring protocol created by inserting two stationary cylindrical baffles into the TRM (Finn & Cox 2001).

create an effective flow topology – the two remaining cylinders can be held stationary as baffles, provided that the moving cylinder loops around them appropriately. This significantly simplifies construction of the device, but it is not clear for general values of m whether the flow topology with the greatest λ_{theory} can always be achieved with $m-1$ stationary cylinders and one cylinder moving by means of simple gearing.

Specifically, in figure 9 we show a cycloidal path $z = p_1(t)$ for one of the cylinders (radius $a_{\text{in}} = 0.1a$), of the form

$$p_1(t)/a = -0.1 + 0.2\exp(2\pi \mathrm{i}t/T) + 0.5\exp(4\pi \mathrm{i}t/T) \tag{5.1}$$

(recall that $z = p_1(t)$ is the location of the axis of the cylinder at time t), which can be generated using a simple gearing arrangement (Finn & Cox 2001). When the BSD contains only one cylinder, we have elsewhere named it the translating rotating mixer (TRM). By adding two further stationary cylindrical baffles, each of radius $a_{\text{in}} = 0.05a$, with axes fixed at $p_2 = -0.2a$ and $p_3 = 0.4a$, we obtain a flow with the topology of the braid $\sigma_2^{-1}\sigma_1^{-1}\sigma_1^{-1}\sigma_1^{-1}\sigma_1^{-1}\sigma_2^{-1}$ (see figure 9); according to the theory outlined in § 3.2, this protocol has $\lambda_{\text{theory}} = 3 + 2\sqrt{2} \approx 5.8$. Despite the presence of baffles leading to topological chaos (see figure 10), we find that $\lambda_{\text{num}}^{\text{BSD}}$ only slightly exceeds $\lambda_{\text{num}}^{\text{TRM}}$ (by less than 10% in our viscous model).

Such a gain may be worthwhile provided the energy costs are not too great. We therefore now consider the energy input required to operate the device in the viscous model. We would expect the introduction of baffles into the TRM to increase its energy consumption, and we now seek to quantify this effect. The force $\mathscr{F}_j$ exerted by the jth cylinder on the fluid is readily determined to be $4\pi\mu\mathrm{i}b_{j,1}$ (Milne-Thomson 1968), and the moment $\mathscr{M}_j$ about the axis of the jth cylinder that it exerts on the fluid is $-4\pi\mu c_{j,1} - \mathrm{Im}\,(\mathscr{F}_j \bar{p}_j)$, where μ is the dynamic viscosity of the fluid. The corresponding force $\mathscr{F}_{\text{out}}$ and moment $\mathscr{M}_{\text{out}}$ about the origin exerted by the outer cylinder on the fluid are

$$\mathscr{F}_{\text{out}} = -4\pi\mu\mathrm{i}\sum_{j=1}^{m} b_{j,1}, \quad \mathscr{M}_{\text{out}} = 4\pi\mu\sum_{j=1}^{m} c_{j,1}. \tag{5.2}$$

The total power input $\mathscr{P}$ to the BSD is then

$$\mathscr{P} = \mathscr{M}_{\text{out}}\Omega_{\text{out}} + \sum_{j=1}^{m}\left(\mathscr{F}_j^x U_j + \mathscr{F}_j^y V_j + \mathscr{M}_j\Omega_j\right). \tag{5.3}$$

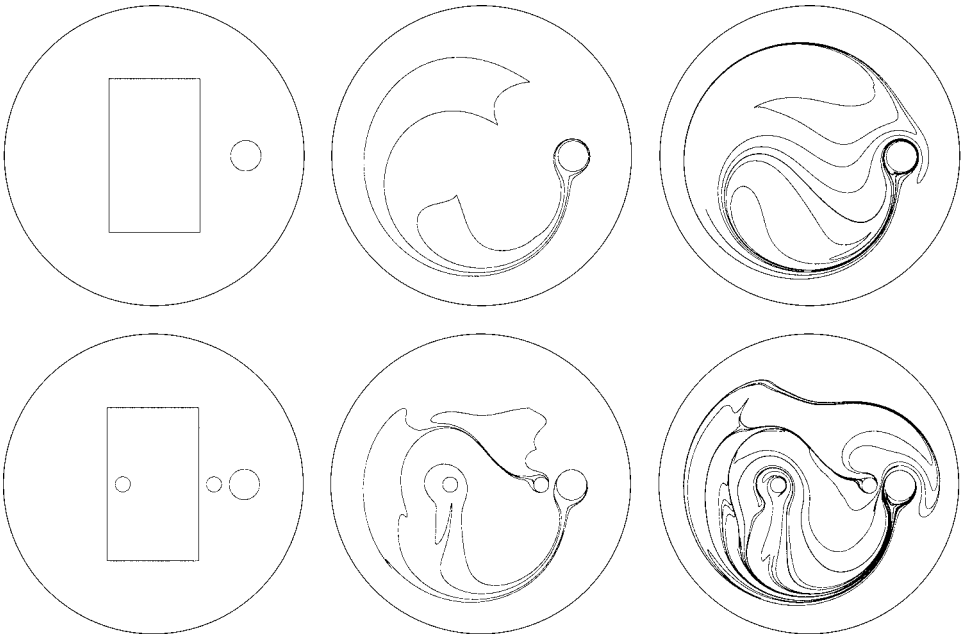

FIGURE 10. Numerical dye-advection plots for the TRM (top row) and BSD (bottom row) after 0, 1 and 2 periods. Apart from the presence of two additional stationary cylinders in the BSD, the two stirring motions are otherwise identical (see figure 9).

Using these results, we calculate that approximately 400% more energy is required with the baffles in place. The quantitative details of the improvement in stretch rate and the excess energy consumption depend sensitively on the size and location of the additional cylinders, and the balance between the two would form an interesting future study. However, it is clear in this case that a marginal improvement in stretching is obtained only at great energetic cost.

Three broader issues, related to the energetics of the BSD, would influence a more ambitious project designed to identify some optimal stirring protocol (using least energy, say). First, once we have selected a protocol with a given topology, it remains to tune parameters such as a_{in} and r. Simple reasoning shows that these can significantly affect the energy requirements of the device, for if the internal cylinders lie close together then the power input is large and the region of good mixing is presumably correspondingly small. Alternatively, when the internal cylinders lie far apart, their proximity to the outer boundary becomes significant, and once again the power input becomes large. We anticipate that for a given set of internal cylinders there exists some optimum way to execute a given braid motion, for minimum energy input. Secondly, we note that when $m = 3$, the same energy is required to execute any of the braid letters σ_1, σ_1^{-1}, σ_2, σ_2^{-1} using the motions described in § 3.2 (this is clear by symmetry). However, when $m > 3$, cylinder exchanges taking place closer to the outer boundary require more energy than those further away, so the choice of braid word itself can influence energy usage. The third consideration, alluded to in § 2.2, is that in addition to translating the internal cylinders, we may also rotate them about their respective axes (or, indeed, the external cylinder about its axis), in an attempt to reduce the power input during cylinder exchanges.

6. Conclusions

We have examined through numerical simulation the generation of 'topological chaos' in a batch stirring device (Boyland *et al.* 2000). The device consists of a number of stirring rods whose positions are successively interchanged in a 'plaiting' motion, the topology of which is alone sufficient to determine a certain material stretch rate that can be achieved in a corresponding two-dimensional chaotic fluid flow. This stretch rate is independent of the fluid properties, and of the exact cylinder motions used to achieve the interchanges.

In any practical implementation of the device, however, the theory does not indicate the actual stretch rate that can be achieved, nor does it indicate the extent of the flow domain in which the greatest stretching takes place. To address such issues, we proposed two models for the fluid velocity field: inviscid and highly viscous. Through a complex series solution, we have been able numerically to simulate stirring protocols with various topologies. Our algorithm is simpler, faster, more accurate and requires less storage than alternative finite-element or finite-difference approaches. We have applied our algorithm to perform dye-advection and stretch-rate calculations, and our results agree well with the stretch rates computed by Boyland *et al.* (2000). Effective topologically chaotic stirring protocols can be realized with a single moving stirring rod that loops around other stationary rods, which act as baffles, and this kind of motion can be achieved using simple gearing. However, in a flow examined above, the additional stretching is achieved only at great energetic cost.

The series approach implemented here is readily adapted for stirring elements whose cross-section is not circular, by applying an appropriate local conformal mapping from each non-circular cross-section to a circle. This mapping then modifies the form of the corresponding terms in the expression for the streamfunction (Driscoll & Trefethen 2002). We have in this manner carried out preliminary simulations for stirring elements of both smooth (elliptical) and non-smooth (flat, paddle-like) cross-section (cf. Saatdjian, Midoux & André 1994; Saatdjian & Midoux 1996, for the former). However, even for stirring rods of circular cross-section, our series do not straightforwardly generalize to finite Reynolds numbers, in which case other approaches are necessary (see Vikhansky 2003).

Finally, we note that it is possible to adapt our series approach to three-dimensional flow in a 'static' mixer consisting of a straight pipe containing three (or more) solid tubes, which form a braid down the length of the pipe; fluid becomes mixed as it travels down the pipe (see Boyland *et al.* 2000). Work is in progress to determine how to arrange the internal tubes to achieve the most effective mixing.

Matthew Finn is supported by an EPSRC studentship. We are grateful to Mike Clifford for discussing with us the practicalities of the BSD, and to Hassan Aref for suggesting that we examine this problem. We are particularly indebted to Nick Trefethen for generously donating his time and expertise in complex-variable techniques and Matlab.

REFERENCES

Acheson, D. J. 1996 *Elementary Fluid Dynamics*. Clarendon.

Aref, H. & Balachandar, S. 1986 Chaotic advection in a Stokes flow. *Phys. Fluids* **29**, 3515–3521.

Aref, H. & Jones, S. W. 1989 Enhanced separation of diffusing particles by chaotic advection. *Phys. Fluids* A **3**, 34–38.

Avudainayagam, A. & Jothiram, B. 1988 A circle theorem for plane Stokes flows. *Q. J. Mech. Appl. Maths* **41**, 383–393.

Bourot, J.-M. 1969 Sur l'application d'une méthode de moindre carrés à la résolution approchée du problème aux limites, pour certaines catégories d'écoulements. *J. Méc.* **8**, 301–322.

Boyland, P. 2002 Fluid mechanics and mathematical structures. In *An Introduction to the Geometry and Topology of Fluid Flows* (ed. R. L. Ricca), pp. 105–134. Kluwer.

Boyland, P., Stremler, M. & Aref, H. 2003 Topological fluid mechanics of point vortex motions. *Physica* D **175**, 69–95.

Boyland, P. L., Aref, H. & Stremler, M. A. 2000 Topological fluid mechanics of stirring. *J. Fluid Mech.* **403**, 277–304.

Butler, J. P. & Tsuda, A. 1997 Effect of convective stretching and folding on aerosol mixing deep in the lung, assessed by approximate entropy. *J. Appl. Phys.* **83**, 800–809.

Clifford, M. J., Cox, S. M. & Roberts, E. P. L. 1998 Lamellar modelling of reaction diffusion and mixing in a two-dimensional flow. *Chem. Engng J.* **71**, 49–56.

Clifford, M. J., Cox, S. M. & Roberts, E. P. L. 2000 The influence of a lamellar structure upon the yield of a chemical reaction. *Inst. Chem. Engrs* **78**, 371–377.

Driscoll, T. A. & Trefethen, L. N. 2002 *Schwarz–Christoffel Mapping*. Cambridge University Press.

Finn, M. D. & Cox, S. M. 2001 Stokes flow in a mixer with changing geometry. *J. Engng Maths* **41**, 75–99.

Frazer, R. A. 1925 On the motion of circular cylinders in a viscous fluid. *Phil. Trans. R. Soc. Lond.* A **225**, 93–130.

Giona, M. & Adrover, A. 2001 Global geometry and coarse-grained formulation of the evolution of pointwise intermaterial interface measure in chaotic flows. *Chem. Engng Sci.* **56**, 3387–3399.

Jana, S. C., Metcalfe, G. & Ottino, J. M. 1994 Experimental and computational studies of mixing in complex Stokes flows: the vortex mixing flow and multicellular cavity flows. *J. Fluid Mech.* **269**, 199–246.

Jones, S. W., Thomas, O. M. & Aref, H. 1989 Chaotic advection by laminar flow in a twisted pipe. *J. Fluid Mech.* **209**, 335–357.

Krasnopolskaya, T. S., Meleshko, V. V., Peters, G. W. M. & Meijer, H. E. H. 1999 Mixing in Stokes flow in an annular wedge cavity. *J. Mech.* B/*Fluids* **18**, 793–822.

Kusch, H. A. & Ottino, J. M. 1992 Experiments on mixing in continuous chaotic flows. *J. Fluid Mech.* **236**, 319–348.

Lamb, H. 1932 *Hydrodynamics*, 6th edn. Cambridge University Press.

Macagno, E. O. & Christensen, J. 1980 Fluid mechanics of the duodenum. *Annu. Rev. Fluid Mech.* **12**, 139–158.

MacKay, R. S. 2001 Complicated dynamics from simple topological hypotheses. *Phil. Trans. R. Soc. Lond.* A **359**, 1479–1496.

Meleshko, V. V., Galaktionov, O. S., Peters, G. W. M. & Meijer, H. E. H. 1999 Three-dimensional mixing in Stokes flow: the partitioned pipe mixer problem revisited. *Eur. J. Mech.* B/*Fluids* **18**, 783–792.

Metcalfe, G. & Ottino, J. M. 1994 Autocatalytic processes in mixing flows. *Phys. Rev. Lett.* **72**, 2875–2878.

Milne-Thomson, L. M. 1968 *Theoretical Hydrodynamics*. Macmillan.

Muzzio, F. J., Alvarez, M. M., Cerbelli, S., Giona, M. & Adrover, A. 1999 The intermaterial area density generated by time- and spatially periodic 2D chaotic flows. *Chem. Engng Sci.* **55**, 1497–1508.

Muzzio, F. J. & Ottino, J. M. 1989 Dynamics of a lamellar system with diffusion and reaction: scaling analysis and global kinetics. *Phys. Rev.* A **40**, 7182–7192.

Muzzio, F. J. & Ottino, J. M. 1990 Diffusion and reaction in a lamellar system: self-similarity with finite rates of reaction. *Phys. Rev.* A **42**, 5873–5884.

Muzzio, F. J. & Swanson, P. D. 1991 The statistics of stretching and stirring in chaotic flows. *Phys. Fluids* A **3**, 822–834.

Pollicott, M. & Yuri, M. 1998 *Dynamical Systems and Ergodic Theory*. Cambridge University Press.

Prakash, S. & Kokini, J. L. 2000 Estimation and prediction of shear rate distribution as a model mixer. *J. Food Engng* **44**, 135–148.

Price, T. J., Mullin, T. & Kobine, J. J. 2003 Numerical and experimental characterization of a family of two-roll-mill flows. *Proc. R. Soc. Lond.* A **459**, 117–135.

Ricca, R. L. & Berger, M. A. 1996 Topological ideas and fluid mechanics. *Physics Today* December, 28–34.

Rudman, M., Metcalfe, G., Brydon, A. & Graham, L. 2001 Numerical mixing experiments in the rotated arc mixer (RAM). In *Proceedings of the 6th World Congress of Chemical Engineering*.

Saatdjian, E. & Midoux, N. 1996 Chaotic mixing and heat transfer between confocal ellipses: experimental and numerical results. *Phys. Fluids* **8**, 677–691.

Saatdjian, E., Midoux, N. & André, J. C. 1994 On the solution of Stokes' equations between confocal ellipses. *Phys. Fluids* **6**, 3833–3846.

Sawyers, D. R., Sen, M. & Chang, H. 1996 Effect of chaotic interfacial stretching on bimolecular chemical reaction in helical-coil reactors. *Chem. Engng J.* **64**, 129–139.

Sen, S. K. 1989 Circle theorems for steady Stokes flow. *Z. Angew. Math. Phys.* **40**, 139–145.

Tufillaro, N. B., Abbot, T. & Reilly, J. 1992 *An Experimental Approach to Nonlinear Dynamics and Chaos*. Addison Wesley.

Vikhansky, A. 2003 Simulation of topological chaos in laminar flows. *Chaos* (submitted).

Zumbrunnen, D. A. & Inamdar, S. 2001 Novel sub-micron highly multi-layered polymer films formed by continuous flow chaotic mixing. *Chem. Engng Sci.* **56**, 3893–3897.